2009 Fifth International Conference on Signal Image Technology and Internet Based Systems

Image dependent spatial shape error concealment for multiple shapes

Ferdous Ahmed Sohel and Mohammed Bennamoun
School of Computer Science and Software Engineering
The University of Western Australia
Crawley, WA 6009, Australia
Ferdous.Sohel@csse.uwa.edu.au, m.bennamoun@csse.uwa.edu.au

***Abstract*— Existing shape error concealment techniques consider a single closed shape at a time. However, in many applications there are commonly multiple shapes in a scene/object and they are not necessarily closed. Existing techniques attempt to conceal errors whenever they find a decoded shape is broken. However, in a multiple shape context, it is not that straightforward, as it becomes crucial to determine whether a segment is broken due to data losses or just the beginning of a new segment. This paper presents an *image dependent shape-error concealment technique for multiple shapes* (ISCM) which exploits textural information using a *rubberband* function to determine proper localisation of the shape errors and effectively recover them. Comparative experimental results analysis confirms both a superior error concealment performance and an improved robustness of ISCM technique.**

Keywords- Error concealment; shape coding; video coding; image processing.

I. INTRODUCTION

Many communication channels suffer from a high propensity for error and the resulting impact is compounded as the transmitted bitstreams are generally highly compressed. The influence of these errors can be further aggravated due to error propagation as predictive and variable length coding techniques are frequently used. *Error resilience* techniques have become popular for their ability to tolerate data losses, while maintaining an acceptable subjective shape quality. *Error concealment* is a widely adopted post processing error resilience strategy, where the decoder plays the pivotal role of error masking by attempting to generate a perceptually acceptable approximation of the original data using available data [15].

Error concealment techniques can be broadly classified into two categories: temporal and spatial. Temporal techniques exploit the interframe correlations in a sequence of frames to mask lost pixels in a frame by using data from already correctly received and previously concealed pixels [4, 10, 14]. These techniques have the advantage of having access to past information and therefore can perform well in a video sequence where an object's shape changes very little between consecutive frames. In contrast, when shape information changes significantly, including the emergence of new objects and object occlusion between frames, temporal methods alone are inadequate [13] and also obviously they are not the most appropriate for still images. In these circumstances spatial techniques are preferable, where the strong neighbouring interpixel *spatial correlation* is exploited to conceal erroneous pixels using information from correctly received and previously concealed pixels within a frame [11].

Among the existing spatial shape-error concealment techniques, the *maximum a posteriori* (MAP) estimator combined with a Markov random field has been designed for binary shape representations [12]. This exploits spatial redundant information on a statistical basis, though it does not use shape as a salient feature and so has subsequently been outperformed by those approaches which incorporate shape characteristics [11]. They employ parametric curves to geometrically conceal a lost boundary from correctly decoded shape information, with Bezier curves [4, 13] and Hermite splines [11] used to conceal errors, though neither has information available upon the lost parts of the contour and so depends upon just decoded shape data. Since the control points for these curves are calculated from the tangents at the two contour-ends associated with each lost segment, their performance is highly dependent on the respective tangent vectors. Since the available contours and tangents in particular, may not be representative of the lost contour, this can lead to ineffectual concealment.

These techniques mask spatial shape errors independently of image information. While this may be effective in MPEG-4 based applications where shape is treated separately from texture and motion, they certainly do not provide the best solutions for a wide range of applications in which the shape is used as metadata to describe image/video content. This is because the high spatial correlation between the shape and its underlying image is not exploited. *Image-dependent shape coding and representation* [6], content-based image retrieval [2] and sketch-based queries using an image map to define hyperlinked objects in hyperlinked TV [3] are some examples of possible applications. In these cases, shape is dependent upon the underlying image/video content and hence, the image is usually either transmitted together with the shape or accessed from an available image database at the decoder [6]. In both circumstances the received shape information may be corrupted due to data loss, so image information can be fully used for error concealment

978-0-7695-3959-1/09 $26.00 © 2009 IEEE
DOI 10.1109/SITIS.2009.36

purposes. Based on this a new *image-dependent spatial shape-error concealment* (ISEC) algorithm that utilises the image intensity gradient alongside relevant shape information has been presented in [15].

The aforementioned shape error concealment techniques [4, 11-13, 15] only consider a single closed shape at a time. Consequently, application scenarios with multiple shapes (both closed and open ended) for example, palmprint representations, are not addressed. If there is a broken part in the shape, the single and closed shape based strategies have the advantage that they can solely try to join the broken part using their respective principles. With multiple shapes, another major challenge emerges: whether the broken part of the shape is due to a data loss or that indicates the starting point of another shape. Moreover, since the shapes are not always closed, there may be data losses at their open ends. This paper addresses these issues by proposing a novel technique, namely *image dependent shape error concealment in a multi-shape context (ISCM)*. To exploit image information, ISCM employs the efficient rubberband function [7] which detects the contour from the underlying image gradient data. Whenever a corrupted shape is received at the decoder, the correctly available part is decoded. ISCM considers each discontinuous segment whether it is a part of another segment or a separate one. This is called error localisation. After error localisation, ISCM matches the couples of the contours so that the correct pairs are matched together in cases the shape segments are part of a shape. Once the correct coupling is obtained, the contour between each pair is recovered using the rubberband function. The performance of ISCM has been rigorously tested upon a number of popular test sequences with experimental results confirming its superior error concealment performance compared with existing techniques for both single shape and multiple shapes applications.

The remainder of the paper is organised as follows: Section II presents a brief review of the *rubberband* function as this forms an integral part of the ISCM technique, while Section III describes the complete theoretical model for ISCM. Section IV analyses the experimental error concealment performance of ISCM, with Section V providing some concluding comments.

II. THE RUBBERBAND FUNCTION

The rubberband function was originally proposed for image segmentation [7] and subsequently used as an object selection tool in [8], in shape coding [6] and shape error concealment [15] applications. It is a boundary detection function that performs a greedy search to maximise the total image gradient along the resulting contour. The transition between the foreground and background in an image generally creates abrupt changes in pixel intensity along an object shape-contour [9]. This results in high image intensity gradients for those pixels forming the boundary, which is a valuable marker for missing contour recovery. An illustrative example of the image intensity gradient along the contour of a shape is presented in Fig. 1. It shows the image gradient information (Fig. 1(a)) along the contour in the region of interest (RoI, Fig. 1(b)). It is thus suitable for shape error concealment since the image intensity gradient is high along an object's contour [6].

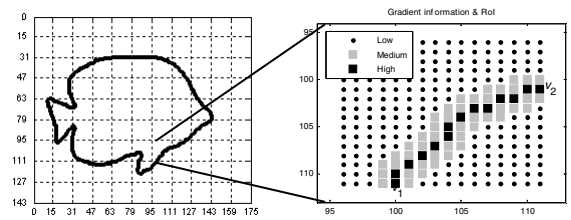

(a) (b)

Fig. 1: Illustration of image intensity gradient along the shape contour – (a) first frame of the Bream sequence, and (b) one macro block with image intensity gradient.

To locate a contour that links the two contour endpoints v_1 and v_2, the rubberband function takes four parameters:

$$(v_1, v_2, w, s) \qquad (1)$$

where s is a scaling factor indicating the kernel size in the image gradient calculations, and w is the width of the rubberband.

A representative illustration of the rubberband is shown in Fig. 2(a). The rubberband function uses a graph search algorithm to detect boundaries. The underlying image in the band defined by the first three parameters of (1) can be considered as a graph, where each pixel is a vertex and an 8-connected neighbourhood is considered for the edges as illustrated in Fig. 2(b). The function comprises two key steps: i) local feature computation and ii) a graph search. In the first step, local image intensity gradients are derived from a scalable edge detector, with this gradient information then being used to define the cost function for having a weighted graph, so for every graph edge $e(p,q)$, where p and q are neighbouring pixels (Fig. 2(b)), the weight/cost $c(p,q)$ is given by:

$$c(p,q) = \frac{1}{\|\nabla_s(q)\| + \delta} \qquad (2)$$

where $\nabla_s(q)$ is the gradient at pixel q with kernel size s and δ is a small positive constant. It this paper the values of s and δ are 4 and 10^{-2} respectively.

Given (2), the image can now be mapped into a weighted and directed graph so the overall rubberband function becomes a shortest-path search algorithm from a source (v_1) to a destination vertex (v_2), which can be solved by a suitable graph search technique, such as the

Dijkstra algorithm where both ends are known (single source single destination shortest path) [5].

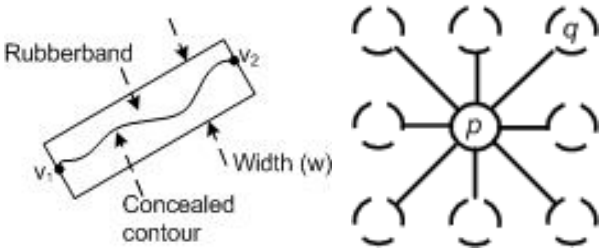

(a) (b)

Fig. 2: (a) Illustration of the rubberband function, and (b) edge definition of the pixel-based graph.

It has however been observed that there are situations where only one end is known and it these cases the Bellman-Ford algorithm (single source multiple destinations shortest path) [5] becomes more appropriate.

III. Image Dependent Shape Error Concealment Technique for Multiple Shapes (ISCM)

The main difference between traditional image-independent (Fig. 3(a)) and image-dependent shape error concealment techniques (Fig. 3(b)) is illustrated via the flowcharts. While the former only exploits available shape information, the ISCM technique utilises both shape and image information.

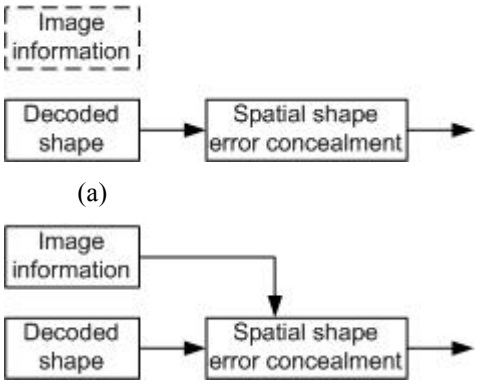

Fig. 3: Shape error concealment approaches: (a) traditional image-independent and (b) Image-dependent.

While both the proposed ISCM and ISEC [15] techniques use image information for shape error concealment purposes, the differences between them is illustrated in Fig. 4. ISEC (Fig. 4(a)) utilizes image information only in its contour recovery module. On the other hand, the proposed ISCM (Fig. 4(b)) technique utilizes image information in three modules: error localization, contour coupling and contour recovery module. It should be noted that the error localisation module is new in ISCM and was not at all present in ISEC. It is an essential module in ISCM as it incorporates the notion of multiple shapes. As shown in Fig. 4(b), the ISCM technique has a number of constituent modules namely: *contour extraction* – to extract the shape-contour from available data; *error localisation* – to determine whether a broken part in the shape is part of a shape or the beginning of a new shape; *contour coupling* – to determine the associated contour endpoints for each lost portion; *contour recovery* – to conceal the shape error by taking image information as an input. Each of these modules is now individually discussed.

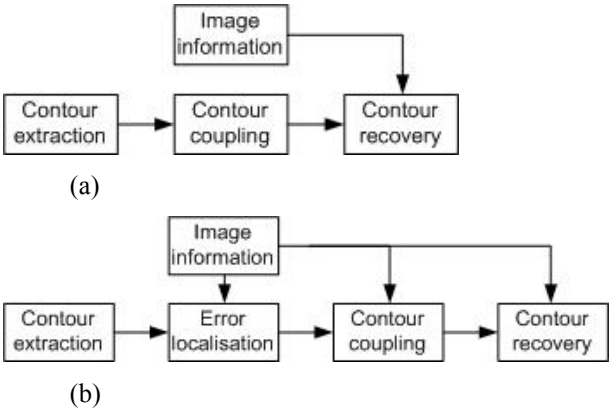

Fig. 4: The difference between ISEC [15] and the proposed ISCM techniques: (a) ISEC and (b) ISCM.

***Contour Extraction*:** This occurs prior to any concealment processing and involves obtaining the correctly decoded contour from the available alpha plane. There are many different contour representations– edge, vertex and shape elements, with an edge based strategy being adopted in this paper due to its inherent robustness [13]. In this representation, the contour is considered to pass between adjacent pixels in a 4-connected neighbourhood with different values. Alternatively, the boundary of an alpha plane is a series of points that belong to the background which has at least one 4-connected neighbour belonging to the object [11]. Fig. 5 presents an illustrative example of the steps of ISCM technique. Fig. 5(a) and (b) respectively present the palmprint shape of the 1st frame of the palmprint database [1][1][1] with data losses in shaded rectangles and the extracted contour.

Error localisation: Since the constraint of a single closed shape has been extended to support the generic case of multiple shapes, it becomes crucial to determine whether a broken part in the shape really represents data losses. This may be due to either data loss or the fact that the original shape is broken. Moreover, the broken parts in the original contour may also become larger due to data losses. The error localisation module checks all these. The main purpose of this module is to determine whether a broken shape segment is part of another segment or it is indeed the beginning of a new segment. The parts of a particular contour are grouped together and labelled accordingly so that they can be effectively used in the contour coupling module. It first selects the first point on the contour. The top

left point amongst the contour ends in the raster scan order is selected as the first point. Then the contour is traced.

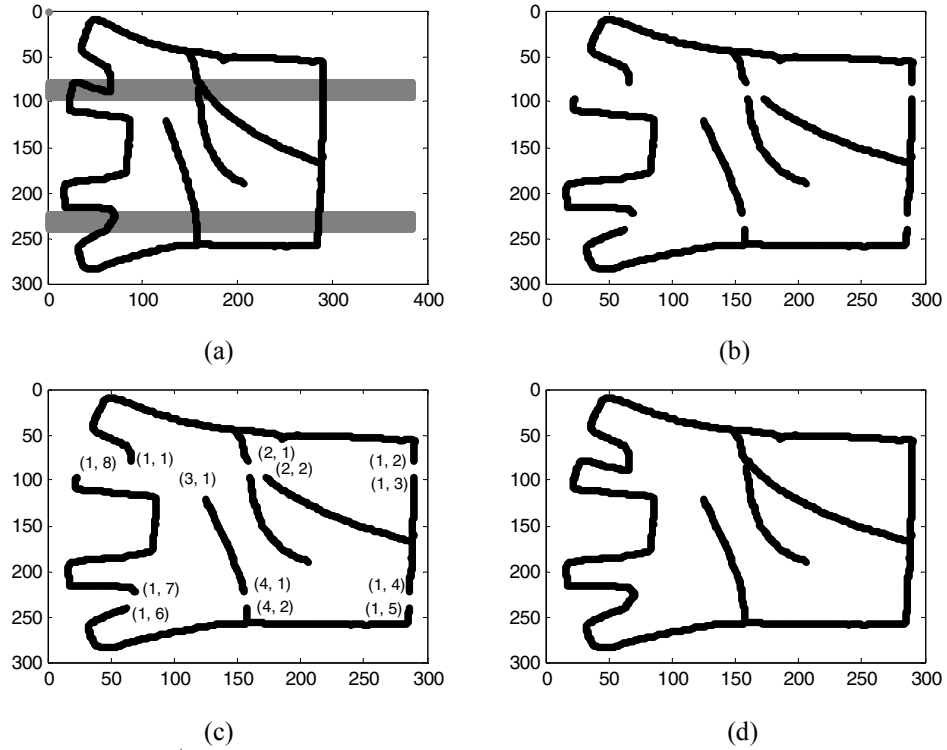

Fig. 5: (a) Shape of 1st frame of the palmprint database with data losses shown in gray blocks. (b) Corresponding extracted contour. (c) Contour labelling and coupling. (d) Recovered shape suing ISCM.

If it finds a discontinuous part at a point of the contour, narrow rubberbands are formed to check if there is a path from this contour end to an end of any other contour with a path cost under a certain threshold, e.g., 5δ, where δ is the rubberband constant shown in (2). If the cost along a candidate contour with endpoints v' and v'' is $C(v',v'')$, $C(v',v'') \le 5\delta$. These rubberbands are formed along the direction of the eight octant lines in the Cartesian coordinate system. It should be noted that the reason of using narrow rubberbands is to speed up the error localisation process. If a valid path is found, it is assumed that they form a continuous contour, though it has been broken due to data losses. These two contour ends are labelled with the same *label_index* and an incremental *end_index* within that label, e.g., (i, j) and $(i, j+1)$ are the two consecutive contour ends for the i th contour. On the other hand, if there is no valid path, there is no more part of this contour and the check then becomes to see if there is any other contour. So the points on this latest contour are removed and the steps above are repeated to find another contour (e.g., *label_index* $i+1$) from the remaining contour points until the contour points set becomes empty. The contour segments of the palm shape of Fig. 5(b) with the proper index and end labelling are presented in Fig. 5(c).

Contour Coupling: The error localization module only localizes the errors and groups the broken segments so that each group represents the parts of a continuous segment. The *coupling* module orders the segment ends in each group with the aim the when they are concatenated, they form a contour closest to the original. While various contour coupling design techniques have been proposed [11, 13], none explicitly combine shape with the underlying textural information. This paper presents a new contour coupling strategy that for the first time integrates texture information relevant to the lost contour, and is formulated by an overall cost function for the rubberband of a concealed contour. If the cost along a candidate contour with endpoints v' and v'' is $C(v',v'')$, then the overall cost function for the entire the $n-$th contour F_n can be expressed as:

$$F_n = \sum_{i \in P_n} C(v',v'')_i \qquad (3)$$

where P_n th contour is the set containing all contour-coupled pairs for each coupling arrangement for the n th contour and i identifies one of the coupled pair in the context of the current coupling arrangement. The coupling which minimises F_n is the final arrangement. The final contour coupling arrangement for the shape is shown in Fig. 5(c). The respective lost data blocks are recorded as *coupled*

image blocks (CIB) along with the associated contour pairs for each missing contour portion. It should be noted that if $|n|$ is the number of segment ends in the n th contour segment, there are $\frac{1}{\frac{|n|}{2}!}\prod_{k=0}^{\frac{|n|}{2}-1}\binom{|n|-2\cdot k}{2}$ combinations in potential coupling pairs, i.e., the number of elements in the set P_n .

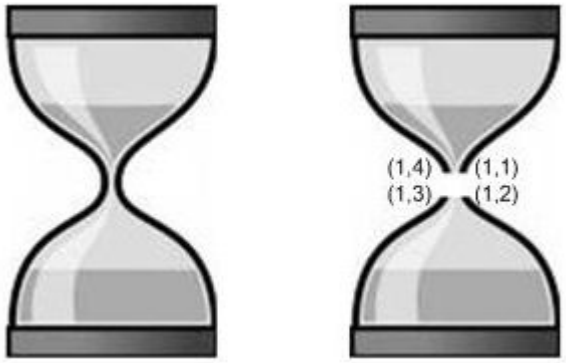

(a) (b)

Fig. 6: Illustration of the advantage of the image dependent contour coupling – (a) the sandclock shape, and (b) example when the textural information plays the perfect role.

The primary reason behind using the rubberband function again in the coupling module is to ensure a correct order of the contour segment ends even in the cases where they are in a very close proximity. For example, the *sandclock* shape shown in Fig. 6(a), the error localization module labels the four broken end points into one segment Fig. 6(b). However, a distance based approach would have resulted in two separate contour segments, i.e., (1, 1) and (1, 4) together and (1, 2) and (1, 3) as the other pair instead of one in the original. Moreover, a tangent based approach [13] would resulted in combination of (1, 1) and (1, 3) as a pair with (1, 2) and (1, 4) as the other pair. On the other hand, the proposed rubberband based approach obtains the correct coupling, i.e., (1, 1) and (1, 2) as one pair with (1, 3) and (1, 4) being the other.

Contour Recovery: Once the error localisation and coupling are performed in a multiple shape context, error recovery becomes the straightforward problem of searching the shortest path based on image gradient between each coupled pair of the shape segments. For this purpose, the error recovery module together with efficient rubberband width measurement techniques proposed in [15] are employed. Two techniques to determine the width of the rubberband were proposed in [15] –Lagrangian optimisation based technique and the computationally fast approximation techniques. In the paper the latter technique is used with a maximum width value of 8 pixels so ISCM is computationally efficient. To emphasise the contribution of this paper with respect to ISEC [15], it should be noted that the proposed ISCM works in a multiple shape context and incorporates texture information into the contour coupling module for better accuracy. Moreover, ISCM is robust enough to deal with shapes which are open ended. For instance, in Fig. 5(c) the shape (with label index 3) has only one end (labelled (3, 1)) in the missing block. It means that the other part of contour is entirely lost. In such cases, Dijkstra based single source single destination shortest path approach is not suitable. A more pragmatic approach would be to use the single source multiple destination Bellman-Ford technique for error recovery. In such cases, the rubberband is formed along the direction of the contour data losses and the furthest vertex in the band with the lowest path cost ($< 5\delta$) is selected as the recovered contour. A set of results are shown in Figure Fig. 5(d).

IV. Results and Analysis

There are a number of different numerical measures that can be effectively used to compare the performance of error concealment techniques. In this paper, the popular *absolute error* (AE), the MPEG-4 distortion measure (D_n) and the *relative error* (RE) metrics are employed, which are also used in [11, 13]. AE is defined as the total number of incorrectly concealed pixels in the alpha plane, while D_n is the ratio of AE to the total number of pixels in the alpha plane. AE is an effective metric to compare the results for different techniques upon the same shape, while D_n provides an insight into the overall proportion of the shape still in error. The third metric RE, which is the ratio of the incorrectly concealed pixels to the total number of lost pixels in the alpha plane [11], reveals the robustness of different techniques to data loss, where (1-*RE*) represents the overall recovered shape that was previously lost. As in other popular shape concealment techniques [11, 13], including MPEG-4 strategies it is assumed whenever data loss occurs, the entire macroblock ($16\times16 pel$) is lost. Fig. 7 shows the data loss model employed in the experiments. When a data packet is received, if the probability of it being dropped is lower than the data loss rate (DLR), the packet is ignored and deemed to be lost data. In Fig. 7, *NL* and *L* represent the *no-loss* and *loss* states respectively.

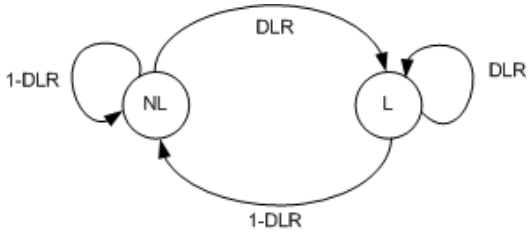

Fig. 7: Schematic diagram of the data loss model.

Table 1: Numerical results for error concealment applied to various shapes and sequences with different error rates.

Test Seq.	DLR	*ISCM technique*			*BC technique [13]*			*HS technique [11]*		
		AE (*pixel)*	D_n (%)	RE (%)	AE (*pixel*)	D_n (%)	RE (%)	AE (*pixel)*	D_n (%)	RE (%)
Bream (QCIF, 300 frames)	5%	06	0.08	1.72	24	0.31	6.86	23	0.30	6.57
	10%	15	0.19	2.15	53	0.68	7.57	54	0.68	7.71
	20%	48	0.62	3.43	160	2.05	11.43	162	2.07	11.57
	40%	132	1.69	9.43	400	5.13	28.57	400	5.12	28.57
Stefan (SIF, 450 frames)	5%	13	0.22	4.51	52	0.9	18.06	51	0.89	17.72
	10%	30	0.53	5.21	124	2.15	21.54	122	2.12	21.19
	20%	74	1.28	6.43	289	5.02	25.1	288	5.00	25.00
	40%	200	3.47	8.69	688	11.95	29.87	680	11.80	29.53
Palmprint (hand geometry) (384×284; 380frames)	5%	02	0.03	0.90	08	0.13	3.60	08	0.13	3.60
	10%	08	0.13	1.50	25	0.42	4.69	24	0.40	4.60
	20%	35	0.59	2.70	60	1.0	4.70	62	1.0.	4.73
	40%	100	1.67	6.02	180	3.0	10.84	180	3.0	10.84
Palmprint (multiple shapes) (384×284; 380frames)	5%	04	0.07	0.95	-	-	-	-	-	-
	10%	11	0.19	1.51	-	-	-	-	-	-
	20%	40	0.70	2.72	-	-	-	-	-	-
	40%	120	2.10	6.05	-	-	-	-	-	-

'–' stands for 'no results are available'.

Table 2: Maximum tolerable DLR for different error concealment techniques, while maintaining a prescribed admissible error (D_n).

Test Seq.	Admissible % error (D_n)	*ISCM*	*BC technique [13]*	*HS technique [11]*
Bream (QCIF)	0.25	12	4	4
	0.5	18	7	7
	1.0	26	12	12
	5.0	55	38	38
Stefan (SIF)	0.25	6	2	2
	0.5	9	3	3
	1.0	15	5	5
	5.0	45	20	20
Palmprint database (hand geometry)	0.25	15	9	9
	0.5	20	12	12
	1.0	30	25	25
	5.0	60	50	50
Palmprint database (multiple shapes)	0.25	14	-	-
	0.5	18	-	-
	1.0	25	-	-
	5.0	50	-	-

The primary contribution of this ISCM technique is that it effectively performs error concealment in the cases where there are multiple shapes in a scene. The existing techniques only work on a single closed shape at a time. A set of experimental results with multiple shapes are presented in Fig. 5(d). It should be noted that the proposed technique uses the image gradient information to determine the most appropriate contour coupling which makes it accurate in cases where the broken contour ends are in a very close proximity (shown in Fig. 6). It should be emphasised that ISCM is equally applicable to single shapes. Extensive experimental tests were conducted to compare ISCM's error concealment performance upon a large variety of shapes.

Table 1 gives the corresponding numerical results upon various test sequences and the *Palmprint* database [1], for DLR values up to 40%. For the *Bream* sequence with a DLR of 10%, the results conclusively demonstrate the improved performance with ISCM, BC and HS techniques generating AE values of 15, 53 and 54 *pixels* respectively, with similar lower error values for ISCM being secured in both the D_n and RE measures. It should be noted that since for a single closed shape ISCM and ISEC produced the same results, only ISCM is shown. Analogous observations can be made for the *Stefan* and *Palmprint* (hand geometry – only the hand outline) results, namely that ISCM sustained lower spatial shape-errors, with the performance becoming especially striking at higher DLR values. This not only confirms the robustness of the new algorithm, but vindicates the rationale of capitalising upon the underlying textural information of lost boundary regions, for error masking purposes. However, when a multiple shape context is the concern, only ISCM can effectively perform error concealment, for instance with a DLR of 5%, AE and D_n produced by ISCM were respectively 4 *pixels* and 0.07%. A further series of experiments were performed to assess the robustness of the ISCM algorithm by investigating the maximum DLR able to be tolerated by each technique, while concomitantly maintaining a prescribed admissible error limit (D_n) following concealment. Table 2 gives the numerical results for various test combinations upon different shapes, which conspicuously evince that in maintaining a prescribed decoded shape quality, ISCM was consistently more relaxed in permitting a significantly greater data loss. For example, in the high motion *Stefan* sequence using a preset admissible error of D_n=1.0%, ISCM tolerated up to 15% DLR at the decoder, while the respective thresholds for both the BC and HS-based strategies were only 5%, thus underscoring the greater robustness ISCM affords by seamlessly incorporating texture information into the concealment process. In a multiple shape context, it was once again found that ISCM can effectively perform error concealment while other techniques did not consider the context of multiple shapes.

V. CONCLUSION

This paper has presented a novel *image dependent spatial shape-error concealment* (ISCM) technique that utilises both shape and the underlying image information for error concealment and effective for application with multiple shapes. ISCM is specifically designed for applications where an object's shape is used as dependent metadata for image descriptive purposes. It conceals shape-errors by exploiting highly correlated image information, with the kernel element being the rubberband function which uses image data to approximate a missing contour. ISCM takes advantages of the image gradient information in error localisation and contour coupling modules as well. Experimental results confirm the superior error-concealment performance of the ISCM approach compared with other existing shape-based techniques and especially its effectiveness in the context of multiple shapes.

ACKNOWLEDGMENT

This work was supported in part by ARC discovery grants (DP0664228 and DP0771294), a University of Western Australia (UWA) postdoctoral fellowship and a UWA research development award. The authors also acknowledge portions of the work were tested on the PolyU Palmprint Database [1].

REFERENCES

[1] PolyU Palmprint Database, http://www.comp.polyu.edu.hk/~biometrics/.

[2] S. Berretti, A. D. Bimbo, and P. Pala, "Retrieval by shape similarity with perceptual distance and effective indexing," IEEE Transactions on Multimedia, vol. 2, no. 4, pp. 225-239, 2000.

[3] V. M. Bove Jr., J. Dakss, E. Chalom, and S. Agamanolis, "Hyperlinked TV research at MIT media laboratory," IBM Systems Journal, vol. 34, no. 3-4, pp. 470-478, 2000.

[4] M.-J. Chen, C.-C. Cho, and M.-C. Chi, "Spatial and temporal error concealment algorithms of shape information for MPEG-4 video," IEEE Transactions on Circuits and Systems for Video Technology, vol. 15, no. 6, pp. 778-783, 2005.

[5] T. H. Cormen, C. H. Leiserson, R. L. Rivest, and C. Stein, Introduction to algorithms, 2nd ed.: The MIT Press, 2001.

[6] H. Luo, "Image-dependent shape coding and representation," IEEE Transactions on Circuits and Systems for Video Technology, vol. 15, no. 3, pp. 345-354, 2005.

[7] H. Luo and A. Eleftheriadis, "Designing an interactive tool for video object segmentation and annotation," in ACM International Conference on Multimedia (MM), Orlando, Florida, USA, 1999, pp. 265-269.

[8] H. Luo and A. Eleftheriadis, "Rubberband: an improved graph search algorithm for interactive object segmentation," in International Conference on Image Processing (ICIP), Rochester, New York, USA, 2002, pp. 101-104.

[9] T. Meier and K. N. Ngan, "Automatic segmentation of moving objects for video object plane generation," IEEE Transactions on Circuits and Systems for Video Technology, vol. 8, no. 5, pp. 525-538, 1998.

[10] G. M. Schuster and A. K. Katsaggelos, "Motion compensated shape error concealment," IEEE Transactions on Image Processing, vol. 15, no. 2, pp. 501-510, 2006.

[11] G. M. Schuster, X. Li, and A. K. Katsaggelos, "Shape error concealment using Hermite splines," IEEE Transactions on Image Processing, vol. 13, no. 6, pp. 808-820, 2004.

[12] S. Shirani, B. Erol, and F. Kossentini, "A concealment method for shape information in MPEG-4 coded video sequences," IEEE Transactions on Multimedia, vol. 2, no. 3, pp. 185-190, 2000.

[13] L. D. Soares and F. Pereira, "Spatial shape error concealment for object-based image and video coding," IEEE Transactions on Image Processing, vol. 13, no. 4, pp. 586-599, 2004.

[14] L. D. Soares and F. Pereira, "Temporal shape error concealment by global motion compensation with local refinement," IEEE Transactions on Image Processing, vol. 15, no. 6, pp. 1331-1348, 2006.

[15] F. A. Sohel, G. C. Karmakar, and L. S. Dooley, "Image-dependent spatial shape-error concealment," in IEEE International Conference on Signal Processing, ICSP-08 Beijing, China: IEEE, 2008, pp. 753-756.